Applied Catalysis B: Environmental 178 (2015) 12–19

Contents lists available at ScienceDirect

Applied Catalysis B: Environmental

journal homepage: www.elsevier.com/locate/apcatb

Ceramic photocatalytic membranes for water filtration under UV and visible light

Chrysoula P. Athanasekou[a], Nikolaos G. Moustakas[a], Sergio Morales-Torres[b], Luisa M. Pastrana-Martínez[b], José L. Figueiredo[b], Joaquim L. Faria[b], Adrián M.T. Silva[b,**], José M. Dona-Rodriguez[c], George Em. Romanos[a], Polycarpos Falaras[a,*]

[a] Division of Physical Chemistry, Institute of Advanced Materials, Physicochemical Processes, Nanotechnology and Microsystems (IAMPPNM), NCSR Demokritos, 15310 Aghia Paraskevi, Attikis, Athens, Greece
[b] LCM—Laboratory of Catalysis and Materials—Associate Laboratory LSRE/LCM, Faculdade de Engenharia, Universidade do Porto, Rua Dr. Roberto Frias, 4200-465 Porto, Portugal
[c] FEAM-Departamento de Química, Universidad de Las Palmas de Gran Canaria, Edificio Central del Parque Científico-Tecnológico de la ULPGC, Campus Universitario de Tafira, 35017 Las Palmas, Spain

ARTICLE INFO

Article history:
Received 13 July 2014
Received in revised form 6 November 2014
Accepted 10 November 2014
Available online 15 November 2014

Keywords:
Ultrafiltration photocatalytic membranes
Titanium dioxide
Graphene oxide
Azo-dye pollutants
Clean water

ABSTRACT

This work demonstrates the efficiency of a hybrid photocatalysis/ultrafiltration process to eliminate or reduce the contents of synthetic dyes in water. The process involves highly active photocatalytic ceramic ultrafiltration (UF) membranes prepared with the deposition of various photocatalysts on the external and internal (pore) surface of UF mono-channel monoliths. A main challenge consists in swapping from the conventional slurry-type photocatalytic purification technology to a novel photocatalytic membrane filtration technology, using the most prominent recently developed TiO_2 based nanomaterials. With this objective, highly hydroxylated anatase TiO_2 was deposited on ceramic monoliths by applying sol–gel (dip-coating) techniques. Novel materials comprising modified TiO_2 nanocrystals covered with an organic shell layer as well as partially reduced graphene oxide-TiO_2 composites were synthesized and stabilized on the monoliths aiming to develop visible light responding catalytic membranes. The photocatalytic filtration experiments took place in a patented water purification device in continuous flow conditions, using methylene blue (MB) and methyl orange (MO) as azo-dye model pollutants, under near-UV/vis and visible light irradiation. Trying to optimize the membrane photocatalytic efficiency we have examined the impact of several parameters related to both the membrane structure and the hybrid photocatalytic/ultrafiltration process including the amount, porosity and surface area of the stabilized photocatalysts as well as the surface charge. The process parameters were mainly related to the pH of the stream under treatment and the type of pollutant. Furthermore, the novel hybrid process was compared to the standard nanofiltration technique in regard to the pollutant removal efficiency and total energy consumption. As a consolidated output, this work proposes a novel photocatalytic membrane, developed via stabilization of organic shell layer covered TiO_2 nanostructures on the internal and external surface of ceramic monoliths, as the most efficient material to be used in hybrid photocatalytic/ultrafiltration water treatment processes.

1. Introduction

Photocatalysts have been extensively used in combination with membrane processes (inorganic [1–3] or polymeric [4]), with the purpose to limit biofouling and prolong the life time of the membrane. Moreover hybrid photocatalysis-ultrafiltration membrane processes have the potential to eliminate one of the most common problems of membrane separation technologies, which is the generation of toxic condensates. In many of the aforementioned applications, photocatalysts are involved in the form of powders

* Corresponding author at: NCSR Demokritos, Institute of Advanced Materials, Physicochemical Processes, Nanotechnology and Microsystems (IAMPPNM), Neapoleos str., Aghia Paraskevi, GR-15310 Attikis, Greece. Tel: +30 2106503644; fax: +30 2106511766.
** Corresponding author at: LCM Laboratory of Catalysis and Materials Associate Laboratory LSRE/LCM, Faculdade de Engenharia, Universidade do Porto, Rua Dr. Roberto Frias, 4200-465 Porto, Portugal. Tel: +351220414908.
E-mail addresses: adrian@fe.up.pt (A.M.T. Silva), papi@chem.demokritos.gr (P. Falaras).

http://dx.doi.org/10.1016/j.apcatb.2014.11.021
0926-3373/

(slurries) in aqueous suspensions [5–7], as a pre-treatment process to water feeding the membrane filtration modules, or as a post treatment stage to the retentate effluent of the membranes. In the first case, stacking and accumulation of the photocatalyst nanoparticles on the membrane surface compromises the permeate flux while in the latter case, there is the need for an additional treatment to separate and recover the photocatalyst particles from the purified retentate.

More recently, photocatalyst powders have been supported on different materials in the form of thin layers, thus overcoming technological issues associated with separation/recovery of the catalyst particles from the liquid-phase [8,9]. However, the photocatalyst immobilization often results in significant loss of photoactivity, mostly due to the consequent reduction of the effective surface area [10]. Micro-, meso- and nanoporous inorganic membranes in the form of monoliths have been used as immobilization substrates. These monoliths are preferred over the conventional polymeric materials, due to their excellent thermal, chemical, and mechanical stability and the possibility of reusability [11,12]. For example, when membranes are developed via dip-coating and sol–gel techniques, a high temperature treatment is further required to render the deposited amorphous layer into the active TiO_2 anatase crystal phase. Chemical stability in terms of UV irradiation and resistance to the concomitant attack by the photogenerated hydroxyl radicals is also mandatory for the application of photocatalytic membranes in processes that combine photocatalysis and filtration. Ceramic membranes, generally, consist of a macroporous substrate that provides mechanical strength for an overlying thin active layer [13,14]. The usual way to develop the active membrane layer is the sequential dip-coating of the substrate into sols composed of different precursor materials, with particles of decreasing size, as one goes from the rough support to the active layer. The purpose of this multi-coating procedure is to eliminate substrate defects [15,16] that undermine the integrity of the active top layer.

The well-known TiO_2 outstanding properties, such as high surface area, relatively low toxicity, photochemical stability, light absorption, charge transport and superior excited state lifetimes, make it the 'photocatalyst of choice' for most applications [17]. Its wide use in commercial scale is mainly due to its significant activity at room temperature, to the fact that organic pollutants are usually completely mineralized to non-toxic substances (no production of recalcitrant intermediates), to its low cost and finally to the possibility of deposition on various substrates (glass, fibers, stainless steel, inorganic materials, sand, activated carbons), allowing continuous operation/re-use. However, an inherent disadvantage of the TiO_2 photocatalyst limiting its multipurpose application is its high band gap (3.2 eV for anatase crystal phase), requiring activation by UV irradiation, which represents about 4% of the solar irradiation reaching the Earth' surface. To overcome this disadvantage, visible-light-active materials and technologies are under deployment, aiming at extending the TiO_2 photoresponse into the visible region thus exploiting larger part of the solar light spectrum. Modification of TiO_2 by anion or metal doping [18–20] or by the combination with carbonaceous materials like carbon nanotubes, fullerenes and graphene oxide has recently showed significant enhancement of the photocatalytic activity of TiO_2 [21,22].

We focused our work on the development of photocatalytic membranes using not only conventional UV-active TiO_2, but also organic shell layer modified [23] and partially reduced graphene oxide-nanostructured TiO_2 composites [21]. These membranes have been tested for photocatalytic organic dye removal, the discharge of which is a considerable source of non-esthetic pollution as well as eutrophication, and can originate dangerous byproducts through oxidation, hydrolysis, or other chemical reactions taking place in the wastewater phase. In the textile industry up to 200,000 t of these dyes are lost to effluents every year during the dyeing and finishing operations, due to the inefficiency of the dyeing process [24]. Unfortunately, most of these dyes escape conventional wastewater treatment processes and persist in the environment as a result of their high stability to light, temperature, water, detergents, chemicals, soap and other parameters such as bleach and perspiration [25]. During the dyeing process it has been estimated that the losses of colorants to the environment can reach 10–50% [26]. With respect to the number and production volumes, azo dyes are the largest group of colorants, constituting 60–70% of all organic dyes produced in the world [27]. They have a wide range of applications in the textile, pharmaceutical and cosmetic industries, and are also used in food, paper, leather and paints. Some azo dyes can show toxic effects, especially carcinogenic and mutagenic events [28,29]. However, environmental legislation obliges industries to eliminate color from their dye-containing effluents, before disposal into water bodies [30]. Textile manufacturers try to convert the traditional "money-wasting" pollution control process to a profitable operation through recycling the water phase of the waste effluent. Dye degradation has therefore received increasing attention as traditional physical techniques (adsorption on activated carbon, ultrafiltration, reverse osmosis, coagulation by chemical agents, ion exchange on synthetic adsorbent resins, etc.) only succeed in transferring the organic compounds from water to another phase, usually solid, thus creating a secondary pollution source. This secondary solid waste product requires further treatment or regeneration of the adsorbent which adds extra costs to the process. Most of the dyes are also stable toward chemical oxidation and resistant toward decolorization by conventional biochemical and physicochemical methods. In real industrial effluents (i.e. of textile industry), salts exist in water together with dyes and many of the recent investigations in the field involving nanofiltration (NF) include the effect of salt concentration on the membrane surface charge and dye rejection efficiency. In the present work, we have applied solely deionized (DI) water as the liquid matrix for the MO and MB pollutants in order to study and validate the visible light photocatalytic efficiency of the membranes without any interference from parameters related to the overall water quality. Taking into account the UF character of the modified TiO_2 membranes, solute rejection due to size or Donnan exclusion are not the dominant mechanisms of pollutants removal and consequently, the effect of dissolved salts can be neglected [31,32].

2. Experimental

2.1. Materials and reagents

The photocatalysts were developed on γ-alumina UF tubular membrane substrates (mono-channel monoliths) possessing glazed ends of 1.5 cm length each. The membranes were provided by Fraunhofer IKTS (Fraunhofer Institute for Ceramic Technologies and Systems, Germany) under the commercial name of Inopor®. They presented nominal pore size of 10 nm, and had a length of 15 cm, ID and OD of 7 and 10 mm, respectively, with the ultrafiltration layer (1.5 μm in thickness) located on their internal side. In addition, two intermediate pore size γ-alumina layers and a rough macroporous α-alumina support composed the entire monochannel monolith. Details on the pore size and volume of the several layers can be found elsewhere [23].

For the evaluation of the photocatalytic efficiency of the membranes, methyl orange (MO—$C_{14}H_{14}N_3NaO_3S$ 99% Sigma–Aldrich) and methylene blue (MB—$C_{16}H_{18}N_3SCl$ 99% Sigma–Aldrich) dyes were used as model water pollutants: The decomposition of the pollutants was determined using a Hitachi U-3010 UV–Visible spectrophotometer through the decrease of the characteristic absorbance peaks of MO (λ_{max} = 466 nm) and MB (λ_{max} = 664 nm).

The concentrations of the solutions used in the photocatalytic tests were 6.4 mg L^{-1} and 2 mg L^{-1} for the MO and MB respectively.

2.2. Membrane development

2.2.1. Organic shell layer modified-nanostructured TiO_2 membrane (N-TiO_2-10)

For the preparation of the modified nanostructured TiO_2 sol, 15 mL of tetrabutyl orthotitanate (Aldrich 97%) were added dropwise into 100 mL of deionized H_2O acidified with nitric acid (1.5 mL). After vigorous stirring for 4 h, 1-propanol (30 mL) was added and the translucent colloidal solution became completely transparent. The solution was left overnight under vigorous stirring and finally 30 g of urea (Merck) were added [20]. The γ-Al_2O_3 membranes with 10 nm pore size, were coated with the surface modified- nanostructured TiO_2 using the dip-coating technique. The glazing at both ends was covered with Teflon tape and then the membrane was dipped into the sol in a vertical position following three successive dip in–pull out cycles at a rate of 15 cm min^{-1}. Our purpose was to deposit the visible light active-TiO_2 catalyst on the shell and lumen side surface of the monolith simultaneously as well as into the pores, in order to enhance the pollutants photo-induced discoloration efficiency by illuminating both membrane surfaces during a filtration process accelerated by photoinduced hydrophilicity. The membrane was heated at a low rate (0.5 °C min^{-1}) to avoid thermal shock and cracking of the membrane up to 400 °C, where it remained for 2 h. The N-TiO_2-10 membrane was weighted before and after calcination and was found heavier by 20 mg (0.033 mg cm^{-2}), due to the deposition of the N-TiO_2 material [33]. SEM measurements at high magnification suffer from charging effects due to the substrate and the γ-alumina layer. As a result the SEM pictures are generally of bad quality and are not considered as publishable. Some low magnification SEM pictures were collected in [33] revealing the γ-alumina and the photocatalytic layers thickness. Furthermore, micro-Raman mapping spectra were collected throughout the cross-section of the membranes presenting entire distribution of the modified titania nanoparticles across.

2.2.2. Reduced graphene oxide-TiO_2 composite membrane (GOT-10)

Natural graphite (99.9995% purity, 20 μm, from Sigma–Aldrich) was used as precursor of graphene oxide (GO). First, graphite oxide was prepared through the modified Hummers method [34,35]. Then, the resulting material was dispersed in a given volume of water and sonicated with an ultrasonic processor (UP400S, 24 kHz) for 1 h. The resulting sonicated dispersion was centrifuged for 20 min at 3000 rpm to obtain a suspension of GO. Then, the reduced graphene oxide-TiO_2 (GOT) composite was synthesized with this GO suspension by liquid phase deposition (LPD) method at room temperature, as described elsewhere [34], using 0.1 mol L^{-1} ammonium hexafluorotitanate(IV)—$(NH_4)_2TiF_6$ (>99.99% Sigma–Aldrich) and 0.3 mol L^{-1} boric acid—H_3BO_3 (>99% Sigma–Aldrich). The material was separated by filtration, washed with water and dried at 100 °C under vacuum for 2 h. The carbon loading (4 wt.%) was selected taking into account the highest photocatalytic activity obtained with this GOT composite in our previous work [34]. Bare TiO_2 was also prepared and treated by the same method, without the addition of any carbon material. An aqueous dispersion containing the corresponding photocatalyst (50 g L^{-1} of GOT or bare TiO_2 as reference material) was used to immobilize the powders on the different ceramic membranes by dip-coating (down/up velocity of 5 cm min^{-1} and dipping time of 30 s). Three layers were applied on the membranes and after each one, the membrane was dried at 120 °C in an oven for 30 min. After that, the coated membranes were treated at 200 °C, with a heating and cooling rate of 1 °C min^{-1} and under a nitrogen atmosphere. "According to our previous work on GOT composites prepared by the liquid phase deposition (LPD) method as a function of GO loading and thermal treatment [34], we have evidenced that post-thermal reduction at a suitable temperature of 200 °C enhances the photocatalytic activity of GOT composites. Based on the Raman analysis of thermally treated GOT composites, we have found that the main effects underlying this enhancement were the improvement of TiO_2 nanoparticle's size and crystallinity and the partial reduction of the GO sheets (inferred from the reduction of the intense GO photoluminescence and the variation of the G and D bands of GO) that further enhances charge transfer between the composite constituents. In this context, the membranes coated with GOT were treated at 200 °C under nitrogen atmosphere in the present work, and during this thermal treatment a partial reduction of GO occurs while anatase TiO_2 particles are exclusively formed." Finally, the ceramic membranes were softly flushed with compressed air in order to remove the particles that are not well-adhered before the use of these membranes in the experiments. The membranes prepared with GOT and with the reference bare TiO_2 material are labeled as "GOT-10" and "ref GOT-10", respectively.

2.2.3. UV-active TiO_2 membrane (ECT-10)

For the preparation of the ECT TiO_2 photocatalyst an ethanol (Panreac 99.5%)–titanium butoxide (Aldrich 97%) solution, 50:3.5 ratio molar, was added drop by drop to a water–ethanol–citric acid (Panreac 99.5%) solution, 50:60.8:0.36 ratio molar. The mixing time was 3 h. After mixing, the final solution was stirred for 30 min and then allowed to age for 48 h. Then, the catalysts were left to dry at 100 °C for 24 h. Several studies focusing on the degradation of phenol [36], diphenhydramine pharmaceutical [37], 2,4-dichlorophenoxyacetic acid herbicide [38] and imazalil fungicide [39] water pollutants have confirmed that this material presents higher photocatalytic efficiency than the commercial TiO_2 benchmark photocatalyst (Evonik P25). For the preparation of the ECT-10 membrane, a similar methodology to that previously described for the GOT-10 and ref GOT-10 membranes was employed.

2.3. Membrane photocatalytic performance evaluation

The hybrid photocatalytic/membrane filtration process took place in a photocatalytic purification device described in detail elsewhere [40]. In brief, the purification device allowed the simultaneous performance of dead-end filtration/photocatalytic tests, with irradiation applied on both surfaces of the monochannel monolith. Near-UV radiation (315–380 nm) with a peak at 365 nm, was applied for irradiating the shell side surface of the monolith at a light irradiance of 2.1 mW cm^{-2}. This irradiation density was achieved by four UV lamps of 9 W (Phillips-UVA (PUVA) PL-S/PL-L) placed at 3 cm from the outer Plexiglas cell of the membrane reactor and sleeved by a cylinder of thick aluminum foil. Four visible lamps of 9 W (Osram DULUX S 9 W/21-840 G23 LUMILUX Cool White), placed at the same distance of 3 cm from the Plexiglas cell were used to achieve a Vis light irradiation density of 7.2 mW cm^{-2}. The lumen side membrane surface was irradiated by means of either an array of 10 UVA miniature LED emitting near-UV radiation (360 to 420 nm) with a peak at 383–392 nm at a light intensity of 0.5 mW cm^{-2} or an array of 6 visible SMD LEDs (OSA-Optolight OLS-336 BA460) emitting at 460 nm at a light intensity of 0.3 mW cm^{-2}. The total flow of polluted water feeding the reactor was 1.5 mL min^{-1} for all the membranes and the filtration was performed in the dead-end mode. The concentration (C) of MO and MB collected from the retentate and permeate sides of the membrane and the concentrations of the feed (C_0) were determined by measuring the visible light absorbance at 466 nm and

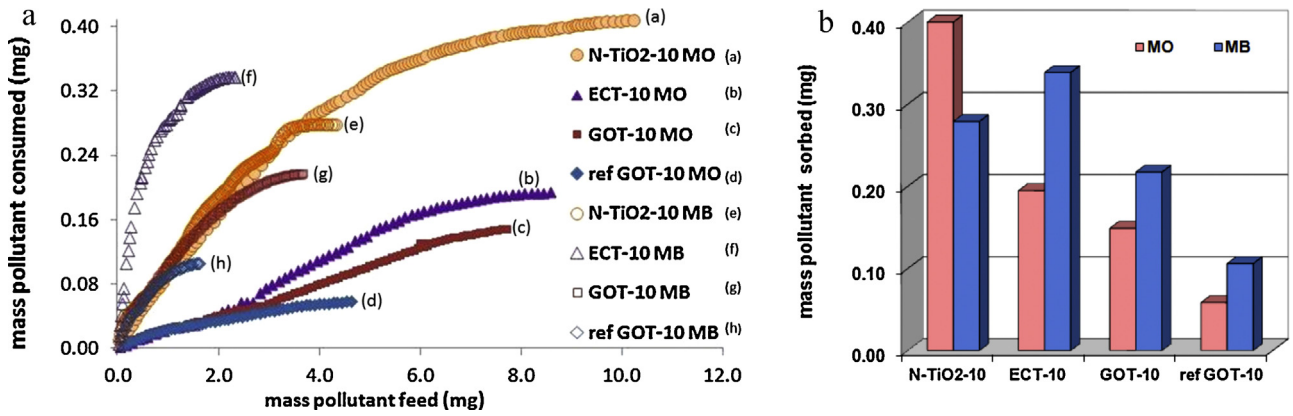

Fig. 1. (a) The adsorbed amount of pollutant vs. the total amount fed in the reactor during dark experiments. (b) The total amount of pollutant adsorbed on each membrane in dark.

664 nm respectively. The total amounts of removed pollutant were obtained from the mass balance between feed and permeate. After each photocatalytic experiment, the cell unit, the piston and the fluid delivery system were washed with deionized (DI) water to ensure that no pollutant species remained in the photocatalytic reactor. The experiments were performed under variable photocatalytic conditions by modifying the fluid flow rate (contact time), the concentration of the pollutant, and the active irradiated surface. This was the first time that a photocatalytic filtration process exploited the action of two active surfaces in one membrane element and the overall concept and way of implementation in an efficient water purification device are already covered by a European patent [41]. Experiments with control samples (unmodified membranes) under irradiation as well as control experiments with modified and unmodified membranes in the absence of irradiation permitted the calculation of the net photocatalytic activity of the two active surfaces developed in each membrane.

3. Results and discussion

3.1. Evaluation of the sorption capacity—Filtration experiments in dark

Filtration experiments were performed sequentially, starting without irradiation (in dark) and the capacity of the two membranes to remove MO (4.4×10^{-3} mg mL^{-1} or 1.49 mol L^{-1}) and MB (1.8×10^{-3} mg mL^{-1} or 0.58 mol L^{-1}) from their aqueous solutions was examined in the dead-end filtration mode (flow-through) with a feed flow of 1.5 mL min^{-1}. Due to the large pore size (10 nm) of the ultrafiltration membranes, mechanisms of size exclusion and charge repulsion of the pollutant molecules can be neglected. However, concentration polarization phenomena can occur when working at the flow-through mode because of the very high water flux through the coated membranes. The thickness of the polarization layer increases as revealed by the plot presented in Fig. 1a, which presents results of the filtration experiments in dark and relates the adsorbed amount of pollutant to the total amount of pollutant fed to the reactor. Filtration experiments in dark had been conducted until the amount of pollutant adsorbed by the unknown amount of the stabilized photocatalyst levels off. Batch adsorption experiments (in dark) of the respective photocatalysts in their powder form were also conducted for the determination of their maximum adsorption capacities (mg g^{-1}) at pH conditions similar to the ones used in the filtration experiments. The ordinate of each point in Fig. 1a was calculated by applying the MO and MB mass balance between the feed and permeate side of the membrane.

The adsorption capacities of the membranes, as derived from the dead-end filtration experiments with MO and MB, divided by the respective adsorption capacities of the photocatalytic powders (mg g^{-1}), gave the amount of photocatalyst which was deposited and stabilized on the ceramic substrates. This amount followed the order: $mass_{(N\text{-}TiO2)} > mass_{(ECT)} > mass_{(GOT)} > mass_{(ref\ GOT)}$ in accordance with the quantities of the adsorbed pollutant as they appear in Fig. 1b. Fig. 1b also reveals that three of the membranes exhibited preferable adsorptivity for MB, the organic shell layer covered TiO_2 membrane being the only exception. The preferable adsorption of MO over MB on this membrane can be explained in terms of point of zero charge (pH_{PZC}) of the involved photocatalysts in relation to the pH of the water solution and the charge of the two pollutants under these conditions. The pH of the used MB solution is 7.2 and the positively charged MB ions (Fig. 2a), are electrostatically attracted by the strongly negative charged surfaces of ECT-10, GOT-10 and ref GOT-10 membranes (namely $pH_{PZC} \approx 5.2$, ≈3.2 and ≈3.5, respectively). On the other hand, at the pH conditions of the MO solution (pH = 6.0 at a concentration of 4.4 mg L^{-1}) the surface of ECT-10, GOT-10 and ref GOT-10 is neutral to negative while MO is also negatively charged since it has lost its amphoteric character due to deprotonation at the —N=N—bridge between the rings (Fig. 2b). This concludes to electrostatic repulsions and limits the amount of adsorbed MO. Regarding N-TiO_2-10 ($pH_{PZC} \approx 6.7$), its surface is positively charged at the pH conditions of the MO solution [42] and as a consequence it attracts the negatively charged MO. On the other hand it is almost neutral at the pH conditions of the MB solution and thus, this explains the higher adsorption capacity for MO compared to MB.

3.2. Photocatalytic filtration experiments under UV irradiation

After the dark period of dye adsorption, the UV irradiation experiments started, with the UV irradiation sources being applied on the lumen and the shell side surfaces of each membrane. The aqueous solution was flowing from the shell to the lumen side. The

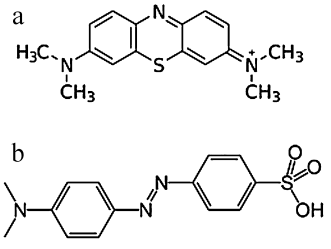

Fig. 2. Molecular formulas of (a) methylene blue and (b) methyl orange.

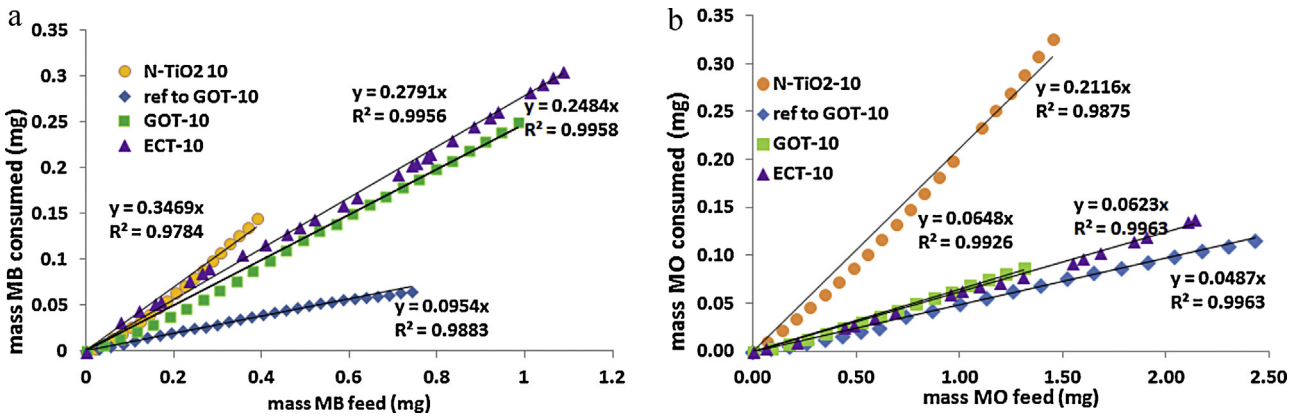

Fig. 3. Mass of pollutant consumed vs. total mass fed in the reactor under UV irradiation: (a) MB and (b) MO.

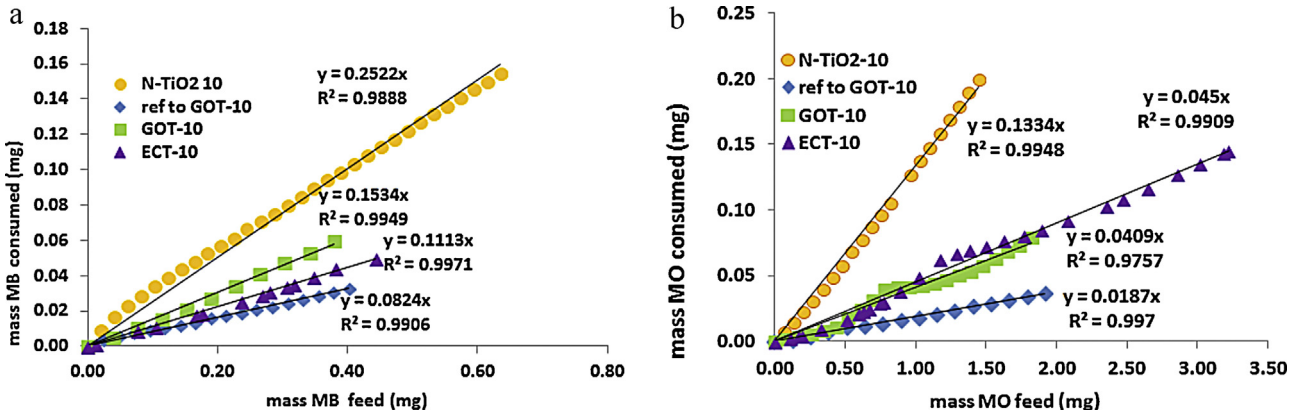

Fig. 4. Mass of pollutant consumed vs. total mass fed in the reactor under Vis irradiation: (a) MB and (b) MO.

corresponding photocatalytically active surfaces of each membrane were approximately 25 and 17.5 cm^2. Fig. 3 represents the amount of pollutant photocatalytically removed versus the total amount fed in the reactor. The slope of the treadlines fitted to the curves is characteristic for the photocatalytic efficiency of each membrane. As seen, the N- TiO_2-10 membrane was the most efficient for the photo-induced discoloration of both MB (Fig. 3a) and MO (Fig. 3b) dyes. The results also show a higher photocatalytic activity of the GOT-10 membrane than that of the reference membrane (ref GOT-10), in particular when using MB. Thus, the addition of GO to TiO_2 favors significantly the discoloration efficiency of the membrane for MB, although it doesn't affect much the photo-induced discoloration efficiency of MO. ECT-10 exhibits similar performances to those of the GOT-10 membrane, under UV irradiation, all the membranes performed better against MB compared to MO. At this point we should stress issues related to the effect of the adsorption capacity on the photocatalytic efficiency of the membranes. It can be seen that the three membranes (ECT-10, GOT-10 and ref GOT-10) presenting higher adsorption capacity for MB exhibited also a 2 to 5-fold higher photocatalytic efficiency for MB compared to MO. On the other hand the N-TiO_2-10 membrane, with higher adsorption capacity for MB than for MO, exhibited almost similar photo-induced discoloration efficiency for both pollutants, even if the MB removal is slightly higher than in the case of MO. Table 1 shows the photocatalytic efficiency (slopes of the plots in Figs. 3 and 4) and the adsorption capacity of the membranes associated with the absolute amount of MO and MB adsorbed and with the photocatalyst characteristics such as the surface area, pore volume, adsorption capacity and point of zero charge (pH_{PZC}).

It can be concluded that amongst the structural characteristics of the deposited photocatalysts, solely the pore volume correlates well with the photocatalytic performance of the membranes. Moreover, the photocatalytic efficiencies correlate well with the absolute amount of the adsorbed pollutant and not with the adsorption capacity ($mg\,g^{-1}$) of each material. The latter unveils that we have achieved the transfer and stabilization of the correct amounts of photocatalysts, thus generating ultra-thin deposits which were fully accessible to the incident irradiation.

Table 1
Characteristic properties of the deposited photocatalysts versus the photocatalytic efficiency of the membranes.

	pH_{PZC}	S_{BET} ($m^2\,g^{-1}$)	Pore vol. ($mL\,g^{-1}$)	Ads.amount (mg)		Ads.capacity ($mg\,g^{-1}$)		Photocatalytic efficiency			
				MO	MB	MO	MB	MO-UV	MO-Vis	MB-UV	MB-Vis
N-TiO2-10	6.7	175	0.46	0.41	0.28	2.8	0.73	0.212	0.133	0.347	0.252
ECT-10	5.2	18	0.25	0.195	0.34	7	1.56	0.062	0.045	0.28	0.111
GOT-10	3.2	110	0.17	0.15	0.22	5.13	1.12	0.065	0.041	0.248	0.153
ref GOT-10	3.5	120	0.11	0.059	0.11	3.6	0.65	0.049	0.019	0.095	0.0824

Table 2
Flow and pressure conditions applied during the photocatalytic filtration experiments and performance characteristics of the developed membranes.

			Rejection efficiency (*R*%)	Permeance ($Lm^{-2}\,h^{-1}\,bar^{-1}$)	Pressure (bar)	Membrane surface area (cm^2)	C/C_0	Energy consumption by the pump ($kW\,h\,100\,m^{-3}$)
GOT-10	MB	Dark	11	17.3	1.7	29.6		4.7
		UV	36	21.2	1.5	30.4	0.65	4.2
		Vis	21	18.2	1.5	31.5	0.77	4.2
	MO	Dark	2	12.4	2.3	29.3		6.3
		UV	7	21.5	1.6	32.8	0.92	4.3
		Vis	5	17.6	1.8	31.5	0.94	5.1
Ref GOT-10	MB	Dark	13	20.5	1.4	27.0		3.9
		UV	14	32.9	1.3	25.1	0.86	3.7
		Vis	12	21.0	1.4	27.2	0.88	3.9
	MO	Dark	2	28.4	1.3	25.1		3.5
		UV	5	39.6	1.2	24.7	0.95	3.2
		Vis	2	31.7	1.1	26.5	0.98	3.2
N-TiO2-10	MB	Dark	9	5.5	5.2	30.8		14.8
		UV	57	8.3	4.6	30.6	0.82	14.6
		Vis	29	9.3	3.7	30.7	0.71	13.9
	MO	Dark	2	7.2	4.5	30.8		12.6
		UV	27	10.8	3.4	30.5	0.95	12.2
		Vis	15	11.6	2.8	30.6	0.97	11.7
ECT-10	MB	Dark	10	2.2	13.5	32.4		37.7
		UV	35	4.2	7.9	32.5	0.64	25.7
		Vis	22	3.8	8.4	32.3	0.84	22.9
	MO	Dark	2	2.8	10.3	32.5		28.7
		UV	7	4.7	8.1	33.0	0.93	27.0
		Vis	5	3.4	9.0	33.0	0.95	25.2

3.3. Photocatalytic filtration experiments under Vis light irradiation

Visible light (Vis-light) filtration experiments were conducted on the membranes after an initial dark step of dye adsorption. The Vis-light irradiation sources were applied on the lumen and the shell side surfaces of each membrane. The preceding results encouraged us to use the organic shell layer covered nanostructured TiO_2 for the development of photocatalytic membranes. In Fig. 4, the slope of each tread line corresponds to the photocatalytic efficiency of the membrane under Vis-light irradiation. As seen, N-TiO_2-10 exhibits a photocatalytic efficiency which is 1.5 and 3 fold higher than those of the other membranes, for MB and MO, respectively, a fact attributed to its narrow band gap (2.19 eV), which makes possible its activation under visible light. The addition of GO to TiO_2 (GOT-10) doubles the performance of TiO_2 alone (ref to GOT-10) for the photo-induced discoloration of both pollutants, indicating that GOT composites with optimal content of GO can extend the photocatalytic activity under Vis-light illumination. The ECT-10 and N-TiO_2 -10 membranes exhibited almost similar photocatalytic performance in the discoloration of MB under UV (Fig. 3a). However, the ECT-10 efficiency for MB removal was moderate under Vis-light (Fig. 4a) showing that the respective photocatalyst is not appropriate for applications in the visible range of the electromagnetic spectrum.

3.4. Comparison of the membranes' performance in terms of pollutant removal efficiency and energy efficiency of the process

The importance of inducing photoactivity on the surface of UF membranes is evidenced by the filtration performance characteristics presented in Table 2 which includes the operation parameters of the photocatalytic filtration process and the efficiency in terms of pollutant rejection efficiency (R%) and capacity to reduce the dyes' concentration (C/C_0) at the permeate effluent.

The pollutant rejection efficiency (*R*%) was calculated according to the following equation:

$$R\% = \frac{C_f - C_p}{C_f} \times 100 \quad (1)$$

where *R*%, the rejection factor, C_f and C_p, the concentration of methyl orange in the feed stream and permeate effluent of the membrane, respectively.

The permeance ($L\,m^{-2}\,h^{-1}\,bar^{-1}$) was calculated according to the following equation:

$$Pe = 9.138 \times 10^{-5} \frac{F_w}{S\Delta P} \times \rho_w \quad (2)$$

where F_w ($mL\,min^{-1}$) the water flow measured at the permeate side of the membrane (inner channel), S (cm^2) the active surface of the membrane, ΔP (atm) the pressure difference between the outer and the inner channel of the reactor and ρ_w the density of water at the temperature of measurement.

The energy consumption ($kW\,h/100\,m^3$) was calculated by means of Eq. (3), in terms of the pump power (shaft power) over the time needed to drive 100 m^3 of water to the membrane module, overcoming in parallel the pressure drop generated on the opposite sides of the membrane during the cross flow filtration.

$$E\,(kW\ \ h) = 100 \times \frac{P \times \rho_w}{S \times 36} \quad (3)$$

In the above equation, P (bar) is the pressure in the retentate side of the membrane, ρ_w ($g\,cm^{-3}$) the density of the fluid and S the pump efficiency (usually 0.8). The performance can also be expressed in terms of permeate pollutant concentration reduction, C/C_0.

The performance characteristics of the membranes during dark filtration (Table 2) are obtained at steady state conditions (i.e. after reaching adsorption equilibrium). All membranes succeed better against MB than MO. When the efficiency of the membranes is evaluated in terms of their capacity to reduce the dyes concentration (C/C_0) at the permeate effluent, the UV irradiation proves to be more effective than Visible, for all the membranes, with the exception of N-TiO_2-10, where the organic layer of the nanoparticles seems to improve the performance against MB, something that does not happen with MO possibly due to the cationic nature of MB. Overall, the best performance comes from the GOT-10 and ECT-10 membranes, which under UV irradiation attain a reduction on the MB concentration of ca. 65% in the permeate relative to the feed.

It can be seen (Table 2) that the permeance values increase, when the membranes are suddenly exposed from filtration in dark

to UV irradiation. This is attributed to the photocatalytic discoloration of the concentrated pollutant that had been accumulated on the external surface (feed surface) of the membrane, upon completion of the adsorption experiment in dark. As already mentioned, irradiation (UV or Vis) is applied to both surfaces of the tubular membrane, aiming to mitigate fouling on the external surface (nano pores) during filtration and to enhance the photoactivity on the internal surface, due to high photocatalyst mass per water volume ratio servicing the elimination of the pollutants from the permeate effluent. The enhanced permeability of the N-TiO_2-10 membrane when irradiated with visible light, compared to UV irradiation, should be highlighted, since it demonstrates the attainment of the desired targeted activation of the catalyst under visible light. The ref GOT-10 appears to be the most hydrophilic material of the four types of TiO_2 used, since this membrane exhibits the highest water flux properties at very low trans-membrane pressures and, therefore, the lowest energy dissipation during operation. Nevertheless, its poor dye removal performance prevents it from being a candidate for UF membrane applications.

The highest pollutant rejection efficiency is achieved using the N-TiO_2-10 membrane against MB and under UV irradiation. ECT-10 and GOT-10 come next, leaving the ref GOT-10 membrane last. The same ranking holds for MO, under both UV and Vis light. Nevertheless, when the energy expense is also considered, N-TiO_2-10 does not appear to be the best choice. GOT-10 can provide 63% of the N-TiO_2-10 membrane's rejection efficiency while consuming only 28% of the respective energy. This means that by recycling the permeate effluent of the GOT-10 membrane back to the reactor two or more times, we can achieve a higher MB or MO rejection efficiency value than that of N-TiO_2-10, with lower total energy consumption.

In any case, the energy consumption values illustrated in Table 2 are, by far, lower than the energy consumption of a typical commercially available ceramic NF membrane which consumes 85 kW h to clean, by size exclusion, 100 m^3 of polluted water, with a MO rejection efficiency of 12%. A typical reverse osmosis (RO) system needs about 120 kW h for the same task. The water recovery of all the photocatalytic membranes tested in this study was 100%, since the experiments were taken place at the "flow through" or "dead end" mode. Contrary, the NF membrane could only participate in "cross flow experiments" [33] with a water recovery of 27 and 32% for the MB and MO experiments, respectively. Operating in the flow through mode and at the same flow rate (1.5 mL/min) would cause enhancement of the pressure above the operation limits of our photocatalytic membrane reactor (50 bar).

When trying to evaluate the economic feasibility of the proposed hybrid photocatalytic/ultrafiltration water treatment process and compare it to the standard NF and RO processes, we should take into account both the energy consumed for powering the UV and Vis irradiation sources and the energy consumed by the pump to circulate the fluid into the reactor. As an example, applying three or more UVA irradiation sources of 8 W each, with the purpose to achieve sufficient irradiation density on the 33 cm^2 of active membrane surface had led to a total energy consumption which was identical to that required by a commercially available polymeric NF membrane process for treating the same amount of water. The reason is that photocatalytic membranes operate not only at much lower pressure but also at higher recovery (100% compared to 30%) [33] and as a consequence, they need less time to treat the same amount of water.

Furthermore, Fig. 5 shows the amount of degraded pollutant (MO and MB) as a function of the energy spent by the process when applying the membrane N-TiO_2-10. As seen, the discoloration of MB due to UV irradiation has an energy cost which is almost double compared to that of MO. Likewise, the visible light discoloration is 1.5 times more expensive when working with MB. In both cases the performance under visible light, is as good as that under UV

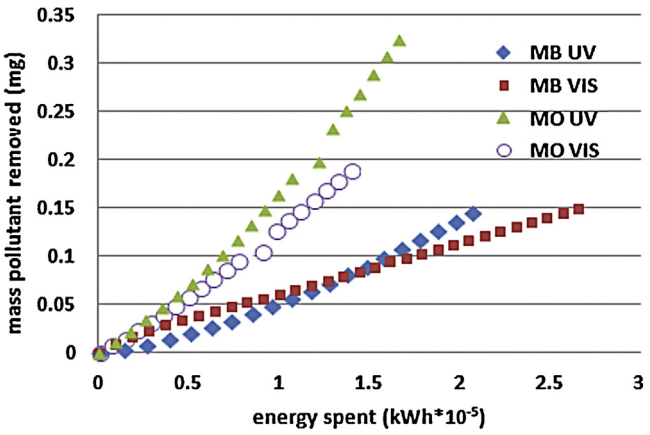

Fig. 5. Degraded pollutant mass by N-TiO_2-10 membrane, under irradiation vs. the corresponding energy consumption (shaft power of the pump).

irradiation and even better for degraded amounts of MB up 0.08 mg. This proves that doping with Nitrogen activates successfully TiO_2 in the visible light fraction of the solar spectrum and the energy cost of employing external UV illumination sources, can be omitted.

It should be also pointed out that the photocatalytic powders used in these studies have shown efficient photocatalytic activity against various other than dye pollutants, (p.e. diphenhydramine [21], cyanobacterial toxins (microcystin LR) and water off-odor compounds (geosmin, 2-methylisoborneol) [43]) both in the UV and visible spectral range. In this study coloured dyes were chosen as the model pollutants due to the facile photometric monitoring of their concentration. Nevertheless, some other compounds of environmental interest which have been proposed by Ryu and Choi [44] for a complete activity assessment of photocatalysis will be examined in the future.

4. Conclusions

Four types of titania modified ultrafiltration membranes were produced via deposition and stabilization of novel photocatalytic materials on the external and internal (pore) surface of ceramic supports. All the membranes proved to be effective against common problems faced by the conventional high flux-thin film composite polymeric nanofiltration systems, when treating waste that contains textile dyes, like fouling tendency, increased energy consumption and the formation of hard-to-dispose toxic concentrate retendate effluents of the pollutant. All membranes performed better against MB than MO. In particular, N-TiO_2-10 proved to be the best membrane for the treatment of MO under UV irradiation and GOT-10 the most appropriate for the treatment of MB. The visible light activation attempts made toward reduction of the energy cost were successful. The proposed combined photocatalytic ultrafiltration process for organic load removal from water exploiting solar light as the only energy source can be effectively applied as an energy efficient alternative to the typical nanofiltration process.

Acknowledgements

This research has been co-financed by the European Union (European Social Fund—ESF) and Greek national funds through the Operational Program "Education and Lifelong Learning" of the National Strategic Reference Framework (NSRF)—Research Funding Program: Thales "AOP-NanoMat" (MIS 379409). Financial support for this work was also provided by project PTDC/AAC-AMB/122312/2010 co-financed by FCT (Fundação para a Ciência e a Tecnologia) and FEDER (ERDF–European Regional Development

Fund) through Programme COMPETE (FCOMP-01-0124-FEDER-019503). This work was also partially co-financed by FCT and FEDER through project PEst-C/EQB/LA0020/2013 (COMPETE). LMPM and SMT acknowledge financial support from FCT grants SFRH/BPD/88964/2012 and SFRH/BPD/74239/2010, respectively, and AMTS acknowledges the FCT Investigator 2013 Programme (IF/01501/2013), with financing from the European Social Fund and the Human Potential Operational Programme.

Appendix A. Supplementary data

Supplementary data associated with this article can be found, in the online version, at http://dx.doi.org/10.1016/j.apcatb.2014.11.021.

References

[1] H. Choi, K. Zhang, D.D. Dionysiou, D.B. Oerther, G.A. Sorial, J. Membr. Sci. 248 (2005) 189–199.
[2] S. Ciston, R.M. Lueptow, K.A. Gray, J. Membr. Sci. 342 (2009) 263–268.
[3] X. Sun, J. Zhang, G. Zhang, X. Pan, T. Huang, Catal. Commun. 18 (2012) 76–80.
[4] S. Mozia, A.W. Morawski, M. Toyoda, M. Inagaki, Sep. Purif. Technol. 63 (2008) 386–391.
[5] K. Nagaveni, G. Sivalingam, M.S. Hegde, G. Madras, Appl. Catal., B: Environ. 48 (2004) 83–93.
[6] V. Kandavelu, H. Kastien, K. Thampi Ravindranathan, Appl. Catal., B: Environ. 48 (2004) 101–111.
[7] N.L. Simantiris, D. Riga, E. Katsivela, D. Mantzavinos, N.P. Xekoukoulotakis, Desalination 250 (2010) 351–355.
[8] R. Comparelli, E. Fanizza, M.L. Curri, P.D. Cozzoli, G. Mascolo, A. Agostiano, Appl. Catal., B: Environ. 60 (2005) 1–11.
[9] C. Guillard, H. Lachheb, A. Houas, M. Ksibi, E. Elaloui, J.M. Herrmann, J. Photochem. Photobiol., A: Chem. 158 (2003) 27–36.
[10] S.-U. Geissen, W. Xi, A. Weidemeyer, A. Vogelpohl, L. Bousselmi, A. Ghrabi, A. Ennabli, Water Sci. Technol. 44 (2001) 245–249.
[11] Y.S. Lin, Sep. Purif. Technol. 25 (2001) 39–55.
[12] L.G.A. van de Water, T. Maschmeyer, Top. Catal. 29 (2004) 67–77.
[13] T.V. Gestel, C. Vandecasteele, A. Buekenhoudt, C. Dortemont, J. Luyten, R. Leysen, B.V.D. Bruggen, G. Maes, J. Membr. Sci. 207 (2002) 73–89.
[14] C.-Y. Tsai, S.-Y. Tam, Y. Lu, J. Brinker, J. Membr. Sci. 169 (2000) 255–268.
[15] A.J. Burggraaf, L. Cot, General overview. Trends and prospects, in: A.J. Burggraaf, L. Cot (Eds.), Fundamentals of Inorganic Membrane Science and Technology, Elsevier, Amsterdam, The Netherlands, 1996, pp. 1–20.
[16] A. Alem, H. Sarpoolaky, M. Keshmiri, J. Eur. Ceram. Soc. 29 (2009) 629–635.
[17] B.G. Kwon, J. Photochem. Photobiol., A: Chem. 199 (2008) 112–118.
[18] M. Pelaez, N.T. Nolan, S.C. Pillai, M.K. Seery, P. Falaras, A.G. Kontos, P.S.M. Dunlop, J.W.J. Hamilton, J.A. Byrne, K. O'Shea, M.H. Entezari, D.D. Dionysiou, Appl. Catal., B: Environ. 125 (2012) 331–349.
[19] C. Han, M. Pelaez, V. Likodimos, A.G. Kontos, P. Falaras, K. O'Shea, D.D. Dionysiou, Appl. Catal., B: Environ. 107 (2011) 77–87.
[20] N.G. Moustakas, A.G. Kontos, V. Likodimos, F. Katsaros, N. Boukos, D. Tsoutsou, A. Dimoulas, G.E. Romanos, D.D. Dionysiou, P. Falaras, Appl. Catal., B: Environ. 130–131 (2013) 14–24.
[21] L.M. Pastrana-Martínez, S. Morales-Torres, A.G. Kontos, N.G. Moustakas, J.L. Faria, J.M. Doña-Rodríguez, P. Falaras, A.M.T. Silva, Chem. Eng. J. 224 (2013) 17–23.
[22] (a) R. Leary, A. Westwood, Carbon 49 (2011) 741–772;
(b) L.M. Pastrana-Martínez, S. Morales-Torres, V. Likodimos, J.L. Figueiredo, J.L. Faria, P. Falaras, A.M.T. Silva, Appl. Catal., B: Environ. 123 (2012) 241–256.
[23] O.C. Vangeli, G.E. Romanos, K.G. Beltsios, D. Fokas, C.P. Athanasekou, N.K. Kanellopoulos, J. Membr. Sci. 365 (2010) 366–377.
[24] H. Zollinger, Synthesis, Properties and Applications of Organic Dyes and Pigments, Color Chemistry, VCH, New York, NY, USA, 1987.
[25] S.R. Couto, Biotechnol. Adv. 27 (2009) 227–235.
[26] H. Ben Mansourr, I. Houas, F. Montassar, K. l Ghedira, D. Barillier, R. Mosrati, L. Chekir-Ghedira, Environ. Sci. Pollut. Res. 19 (2012) 2634–2643.
[27] A. Bafana, S. Saravana Devi, T. Chakrabarti, Environ. Rev. 19 (2011) 350–370.
[28] K.T. Chung, C.E. Cerniglia, Mutat. Res. 277 (1992) 201–220.
[29] H.M. Pinheiro, E. Touraud, O. Thomas, Dyes Pigm. 61 (2004) 121–139.
[30] C. O'Neill, F.R. Hawkes, D.L. Hawkes, N.D. Lourenço, H.M. Pinheiro, W. Delée, J. Chem. Technol. Biotechnol. 74 (1999) 1009–1018.
[31] A. Wahab Mohammad, Sep. Sci. Technol. 37 (2002) 1009–1029.
[32] M. Amini, M. Arami, N.M. Mahmoodi, A. Akbari, Desalination 267 (2011) 107–113.
[33] N.G. Moustakas, F.K. Katsaros, A.G. Kontos, G.Em. Romanos, D.D. Dionysiou, P. Falaras, Catal. Today 224 (2014) 56–69.
[34] L.M. Pastrana-Martínez, S. Morales-Torres, V. Likodimos, J.L. Figueiredo, J.L. Faria, P. Falaras, A.M.T. Silva, Appl. Catal., B: Environ. 123 (2012) 241–256.
[35] W.S. Hummers, R.E. Offeman, J. Am. Chem. Soc. 80 (1958) 1339.
[36] J. Araña, J.M. Doña-Rodríguez, D. Portillo-Carrizo, C. Fernández-Rodríguez, J. Pérez-Peña, O. González Díaz, J.A. Navío, M. Macías, Appl. Catal., B: Environ. 100 (2010) 346–354.
[37] L.M. Pastrana-Martínez, J.L. Faria, J.M. Doña-Rodríguez, C. Fernández-Rodríguez, A.M.T. Silva, Appl. Catal., B: Environ 113–114 (2012) 221–227.
[38] E.I. Seck, J.M. Doña-Rodríguez, C. Fernández-Rodríguez, O.M. González-Díaz, J. Araña, J. Pérez-Peña, Appl. Catal., B: Environ. 125 (2012) 28–34.
[39] D.E. Santiago, J.M. Doña-Rodríguez, J. Araña, C. Fernández-Rodríguez, O. González-Díaz, J. Pérez-Peña, A.M.T. Silva, Appl. Catal., B: Environ. 138–139 (2013) 391–400.
[40] G.Em. Romanos, C.P. Athanasekou, F.K. Katsaros, N.K. Kanellopoulos, D.D. Dionysiou, V. Likodimos, P. Falaras, J. Hazard. Mater. 211–212 (2012) 304–316.
[41] P. Falaras, G., Romanos, P. Aloupogiannis, Photocatalytic Purification Device, European Patent, EP2409954 (A1) –2012-01-25, National Center for Scientific Research Demokritos, Innovative Research & Technology Ltd.
[42] H. Choi, M.G. Antoniou, M. Pelaez, A.A. De La Cruz, J.A. Shoemaker, D.D. Dionysiou, Environ. Sci. Technol. 41 (2007) 7530–7535.
[43] T. Fotiou, T.M. Triantis, T. Kaloudis, L.M. Pastrana-Martinez, V. Likodimos, P. Falaras, A.M.T. Silva, A. Hiskia, Chem. Eng. J. 52 (2013) 13991–14000.
[44] J. Ryu, W. Choi, Environ. Sci. Technol. 42 (2008) 294–300.